

Article

Enhancement of Perfluorooctanoate and Perfluorooctanesulfonate Activity at Acoustic Cavitation Bubble Interfaces

C. D. Vecitis, H. Park, J. Cheng, B. T. Mader, and M. R. Hoffmann

J. Phys. Chem. C, **2008**, 112 (43), 16850-16857 • DOI: 10.1021/jp804050p • Publication Date (Web): 04 October 2008

Downloaded from <http://pubs.acs.org> on December 1, 2008

More About This Article

Additional resources and features associated with this article are available within the HTML version:

- Supporting Information
- Access to high resolution figures
- Links to articles and content related to this article
- Copyright permission to reproduce figures and/or text from this article

[View the Full Text HTML](#)



ACS Publications
High quality. High impact.

The Journal of Physical Chemistry C is published by the American Chemical Society, 1155 Sixteenth Street N.W., Washington, DC 20036

Enhancement of Perfluorooctanoate and Perfluorooctanesulfonate Activity at Acoustic Cavitation Bubble Interfaces

C. D. Vecitis,[†] H. Park,[§] J. Cheng,[†] B. T. Mader,[‡] and M. R. Hoffmann^{*,†}

W. M. Keck Laboratories, California Institute of Technology, Pasadena, California 91125, 3M Environmental Laboratory, 3M Center, Building 260-05-N-17, Maplewood, Minnesota 55144-1000, and School of Physics and Energy Sciences, Kyungpook University, Daegu 702-701, Korea

Received: November 9, 2007; Revised Manuscript Received: August 7, 2008

Acoustic cavitation driven by ultrasonic irradiation decomposes and mineralizes the recalcitrant perfluorinated surfactants perfluorooctanesulfonate (PFOS) and perfluorooctanoate (PFOA). Pyrolytic cleavage of the ionic headgroup is the rate-determining step. In this study, we examine the sonochemical adsorption of PFOX, where X = S for PFOS and A for PFOA, by determining kinetic order and absolute rates over an initial PFOX concentration range of 20 nM to 200 μ M. Sonochemical PFOX kinetics transition from pseudo-first-order at low initial concentrations, $[\text{PFOX}]_i < 20 \mu\text{M}$ to zero-order kinetics at high initial concentrations, $[\text{PFOX}]_i > 40 \mu\text{M}$, as the bubble interface sites are saturated. At PFOX concentrations below 100 μM , concentration-dependent rates were modeled with Langmuir–Hinshelwood (LH) kinetics. Empirically determined rate maximums, $V_{\text{Max}}^{\text{PFOA}} = 2230 \pm 560 \text{ nM min}^{-1}$ and $V_{\text{Max}}^{\text{PFOS}} = 230 \pm 60 \text{ nM min}^{-1}$, were used in the LH model, and sonochemical surface activities were estimated to be $K_{\text{Sono}}^{\text{PFOS}} = 120\,000 \text{ M}^{-1}$ and $K_{\text{Sono}}^{\text{PFOA}} = 28\,500 \text{ M}^{-1}$, 60 and 80 times greater than equilibrium surface activities, $K_{\text{Eq}}^{\text{PFOS}}$ and $K_{\text{Eq}}^{\text{PFOA}}$. These results suggest enhanced sonochemical degradation rates for PFOX when the bubble interface is undersaturated. The present results are compared to previously reported sonochemical kinetics of nonvolatile surfactants.

Introduction

Fluorine is the most electronegative of elements. Fluorochemicals (FCs), organics with the majority of their hydrogens replaced by fluorines, display unique properties as compared to their hydrocarbon analogs.¹ The C–F bond is the strongest among organics ($> 110 \text{ kcal/mol}$), and low C–F bond polarizabilities give them both hydrophobic and oleophobic character. Fluorination protects against oxidation, and FC coatings provide water and oil resistance. However, these same FC properties make them environmentally persistent and recalcitrant toward most conventional water treatment technologies,^{2,3} since they are inert toward common chemical and microbial treatment.^{4–6} Sulfate radical,^{7–9} advanced reduction,^{10,11} and photolytic techniques^{8,12,13} can degrade perfluorinated surfactants, most yielding shorter-chain FCs as products. Moriwaki et al.¹⁴ reported that ultrasonic irradiation of aqueous perfluorochemical solutions may provide a practical alternative.

Acoustic cavitation as driven by ultrasonic irradiation can be utilized for the decomposition of aqueous chemical contaminants.^{15–18} Application of ultrasound to aqueous solutions forms cavitation bubbles, which will undergo transient collapse events.¹⁹ Quasi-adiabatic compression of transient bubbles generates average vapor temperatures near 5000 K^{20,21} and much higher bubble vapor core temperatures that lead to sonoluminescence (SL).^{22,23} Water vapor readily pyrolyzes under the transient high temperatures, producing O-atoms, hydroxyl radicals, and H-atoms.²⁴ Hot vapor colliding with the collapsing bubble wall generates interfacial temperatures of at least 800 K.^{17,24} Chemicals preferentially partitioning to the bubble vapor

will decompose via pyrolytic and combustion reactions.²⁵ Nonvolatile surfactants that are difficult to oxidize, such as perfluorooctanesulfonate (PFOS) and perfluorooctanoate (PFOA), will pyrolytically decompose at the bubble–water interface.¹⁴

Understanding the physical processes that control PFOX (X = S or A) degradation rates is key to optimization of their sonochemical kinetics. PFOX sonochemical degradation involves an initial, rate-determining ionic headgroup cleavage at the bubble–water interface followed by relatively quick mineralization of the fluorocarbon tail.²⁶ However, adsorption of PFOS and PFOA to the bubble–water interface, a physical process required before interfacial sonochemistry can occur, has yet to be investigated.

Henglein and Kormann²⁷ first noted that hydroxyl radical scavenging activity increased with increasing organic chain length at cavitation bubble interfaces. Later, Fyrrillas and Szeri made numerical calculations²⁸ of nonvolatile surfactant adsorption to an oscillating bubble interface. Their model calculations predicted a decrease in the maximum Gibbs surface excess, $\Gamma_{\text{Max,Sono}}$, as compared to the equilibrium max surface excess, $\Gamma_{\text{Max,Eq}}$, due to surface site limitations at bubble radial minimums and an increase in sonochemical surface activity, K_{Sono} , relative to equilibrium surface activity, K_{Eq} , due to high velocity radial oscillations. Concentration dependent sonochemical degradation kinetics of humic materials²⁹ and pesticides³⁰ have been empirically modeled by Langmuir–Hinshelwood (LH) kinetics, suggesting that adsorption to the bubble–water interface is the initial step in their primary sonochemical decomposition mechanism and limiting at high concentrations. Sostaric and Reisz^{31,32} observed saturation of alkyl radical production during concentration-dependent sonolysis of alkyl sulfates and sulfonates. However, alkyl radical production from nonvolatile surfactants of various chain lengths did not correlate well with equilibrium Gibbs surface excess values, Γ_{Eq} . The lack of correlation was

* Corresponding author. E-mail: mrh@caltech.edu.

[†] California Institute of Technology.

[‡] 3M Environmental Laboratory.

[§] Kyungpook University.

concluded to arise from relatively short acoustic bubble lifetimes (100s μ s) as compared to ionic surfactant equilibration times (>1 ms). Tronson et al.³³ observed that Langmuir competitive adsorption modeling using equilibrium sodium dodecyl sulfate (SDS) surface excess values, $\Gamma_{\text{Eq}}^{\text{SDS}}$, did not fit trends expected from SL data. Total acoustic bubble volume measurements as a function of alcohol concentration correlated well with Γ_{Eq} ; however, Γ_{Eq} overestimated sonochemical ionic surfactant adsorption.³⁴ Sonochemical adsorption of nonvolatile (i.e., ionic) surfactants is not well-described by equilibrium partitioning.

Here, we investigate sonochemical PFOS and PFOA adsorption to the bubble–water interface by determining absolute rates over 4 orders of magnitude of initial PFOX concentrations. Sonochemical effects on surface activity, $K_{\text{Sono}}^{\text{PFOX}}$ vs $K_{\text{Eq}}^{\text{PFOX}}$, are evaluated by modeling the concentration-dependent kinetics with the LH formalism using an empirically determined $V_{\text{Max}}^{\text{PFOX}}$ and comparing the results to equilibrium surface partitioning determined by surface tension measurements. Sonochemical PFOX surface activity determined here is compared to previously observed results.

Experimental Methods

Ammonium perfluorooctanoate (PFOA) and sodium perfluorooctanesulfonate (PFOS) were provided by the 3M Corporation. Ammonium acetate ($>99\%$) and methanol (HR-GC, $>99.99\%$) were obtained from EMD Chemicals, Inc. Aqueous solutions were prepared with distilled and deionized water that was further purified using a MilliPore system (18.2 $\text{M}\Omega \cdot \text{cm}$ resistivity).

Ultrasonic irradiation was performed at a frequency of 358 kHz and an applied power density of 250 W L^{-1} with an Allied Signal ELAC Nautik ultrasonic transducer. The average energy transferred to solution was 75%, as determined by calorimetry. The reaction solution was contained in a 600 mL water-jacketed glass reactor. The temperature was controlled with a Haake A80 refrigerated bath maintained at 10 $^{\circ}\text{C}$. All reactions were continuously sparged with argon for 30 min prior to and for the duration of the reaction. PFOS and PFOA were sonicated simultaneously over an initial concentration range of 20 nM to 200 μM . Higher concentrations were not tested, as sonication caused the compounds to precipitate. Concentration versus time profiles were fitted either to a single exponential decay for first-order kinetics, or linearly for zero-order kinetics.

Analysis of PFOA and PFOS was completed by high-performance liquid chromatography mass spectrometry (HPLC-MS). The samples were placed into 750 μL polypropylene autosampler vials and sealed with a poly(tetrafluoroethylene) (PTFE) septum crimp cap. For reactions with initial concentrations greater than 250 ppb, serial dilutions to achieve a concentration of ca. 50 ppb were completed prior to analysis. Aliquots (20 μL) were injected into an Agilent 1100 LC for separation on a Betasil C18 column (Thermo-Electron) of dimensions 2.1 mm i.d., 100 mm length, and 5 μm particle size. A 2 mM aqueous ammonium acetate/methanol mobile phase at a flow rate of 0.75 mL min^{-1} was used with an initial composition of 70:30 water/methanol. Analytical procedures are detailed in previous reports.²⁶ The HPLC effluents were analyzed with an Agilent Ion Trap MS in the negative ion mode for the PFOS molecular ion ($m/z = 499$) and the decarboxylated PFOA ($m/z = 369$). The nebulizer gas pressure was 40 PSI, while the drying gas flow rate and temperature were 9 L min^{-1} and 325 $^{\circ}\text{C}$, respectively. The capillary voltage was set at +3500 V, and the skimmer voltage was -15 V. Quantification was completed by first producing a calibration curve using eight concentrations between 1 and 200 ppb fitted to a quadratic with X^{-1} weighting.

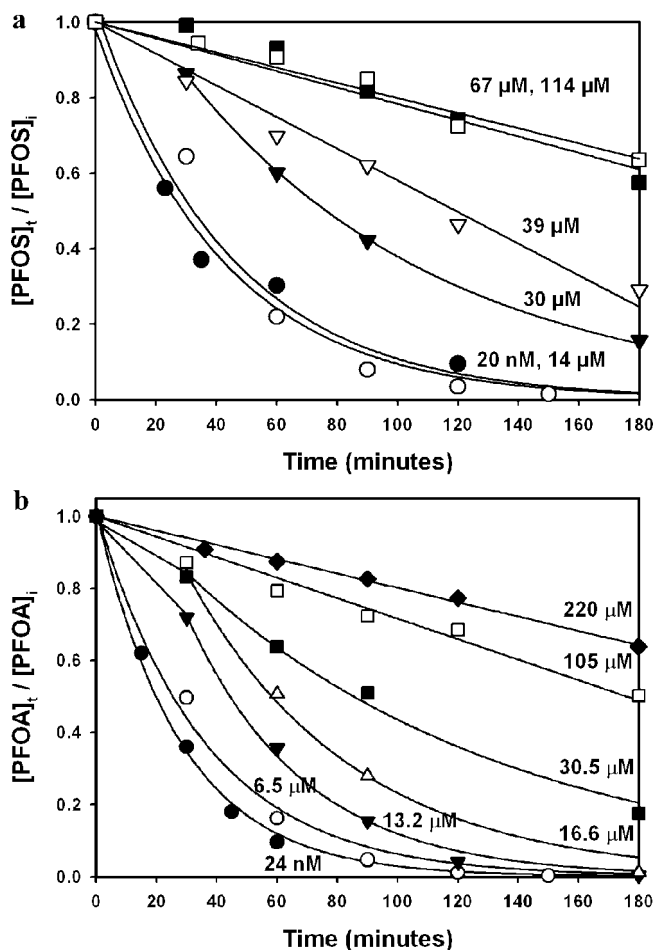


Figure 1. Time-dependent plots of PFOS and PFOA sonolytic degradation over a range of initial concentrations under ultrasonic conditions: 358 kHz, 250 W L^{-1} , 10 $^{\circ}\text{C}$, and argon. (a) $[\text{PFOS}]_t/[\text{PFOS}]_i$ vs time in minutes. $[\text{PFOS}]_i$ = (●) 20 nM, (○) 14 μM , (▼) 30 μM , (▽) 39 μM , (■) 67 μM and (□) 114 μM . (b) $[\text{PFOA}]_t/[\text{PFOA}]_i$ vs time in minutes. $[\text{PFOA}]_i$ = (●) 20 nM, (○) 6.5 μM , (▼) 13.2 μM , (△) 16.6 μM , (■) 30.5 μM , (□) 105 μM and (◆) 220 μM .

Surface tension measurements were made with a De Nouy tensiometer utilizing the standard ring method (ASTM D1331-89). The tensiometer was calibrated with a weight of known mass. Each sample was measured three times with the deviation between measurements less than 1%. The PFOS measurements were completed up to ~ 1 mM, where the compound became insoluble. The curve was fitted to the surface pressure equation of state using Matlab to determine the partitioning coefficient and the maximum surface concentration.

Results

PFOX Concentration-Dependent Sonochemical Kinetics. Sonolysis of aqueous solutions containing both PFOS and PFOA were carried out over a range of initial concentrations from 20 nM to 200 μM ($\nu = 354$ kHz, $\rho_{\text{PD}} = 250$ W L^{-1} , $I = 6.4$ W cm^{-2}). A plot of $[\text{PFOS}]_t/[\text{PFOS}]_i$ vs time for a representative set of PFOS concentrations is shown in Figure 1a. At PFOS concentrations over the range of 20 nM to 14 μM , the observed kinetics are pseudo-first-order over four half-lives and are fitted to a single exponential decay. Previously reported results on PFOS and PFOA sonochemical decomposition completed at $[\text{PFOS}]_i \leq 20$ μM displayed a similar kinetic order.^{14,26} At PFOS concentrations of 39–202 μM , the reaction kinetics are zero-order over the entire time-course. At an intermediate PFOS

TABLE 1: Concentration-Dependent Sonochemical Kinetics

[PFOA] (nM)	first-order (min ⁻¹)	zero-order (M min ⁻¹)	-d[PFOA]/dt (M min ⁻¹)	[PFOS] (nM)	first-order (min ⁻¹)	zero-order (M min ⁻¹)	-d[PFOS]/dt (M min ⁻¹)
20	0.044 ± 0.013		0.88	20	0.025 ± 0.005		0.5
200	0.047 ± 0.002		9.5	200	0.028 ± 0.006		5.5
2000	0.047 ± 0.005		94	2000	0.028 ± 0.005		56
6400	0.028		180	7300	0.023		165
13100	0.026	51	292	14000	0.019		269
16500	0.0184	39	259	16000	0.019	10	254
30000	0.0088	65	230	26400	0.010	56	229
35500		161	161	30200	0.012	69	313
42500		156	156	39000		152	152
105000		273	273	67300		170	170
145000		314	314	116000		250	250
221000		1022	1022	202000		1150	1150

concentration of 30 μM , the data is fit to a quasi-exponential decay after the concentration dropped below 25 μM after 30 min of sonication. The transition from pseudo-first-order kinetics at low concentrations to zero-order kinetics at high concentrations is consistent with saturation kinetics. Initial PFOS sonochemical decomposition occurs pyrolytically at the bubble–water interface; therefore, at high [PFOS]_i, the number of transiently cavitating bubble–water interfacial adsorption sites becomes saturated.

A qualitatively similar transition was observed for the sonolytic degradation of PFOA upon increasing the initial PFOA

concentration. A plot of [PFOA]_i/[PFOA]_i vs time for a representative set of concentrations is shown in Figure 1b. At initial PFOA concentrations over the range of 24 nM to 6.5 μM , the reaction kinetics are pseudo-first-order over at least four half-lives and are fitted to an exponential decay. At higher initial concentrations where [PFOA]_i ≥ 35 μM , the reaction kinetics are zero-order over the entire time-course. At intermediate concentrations of 13.2, 16.6, and 30.5 μM , the reaction kinetics follow an exponential decay after the first 30 min of reaction. The kinetic transition from pseudo-first-order to zero-

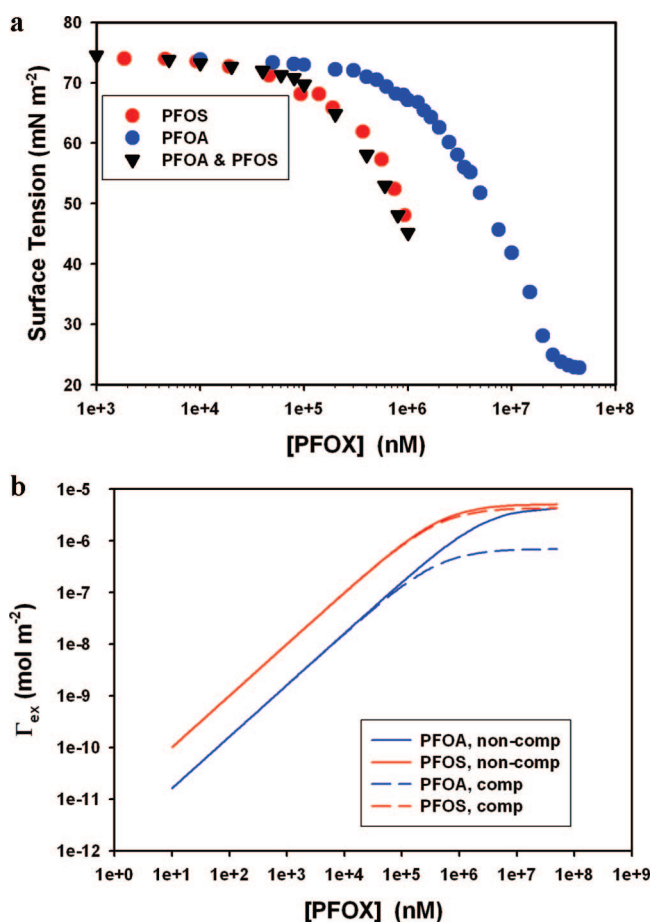


Figure 2. (a) Plot of surface tension vs aqueous PFOS and/or PFOA concentration: (black dot) PFOA, (red dot) PFOS, and (down triangle) PFOS and PFOA. (b) Plot of surface excess vs aqueous PFOS and/or PFOA concentration: (blue solid line) PFOA noncompetitive, (red solid line) PFOS noncompetitive, (blue dashed line) PFOA competitive, and (red dashed line) PFOS competitive.

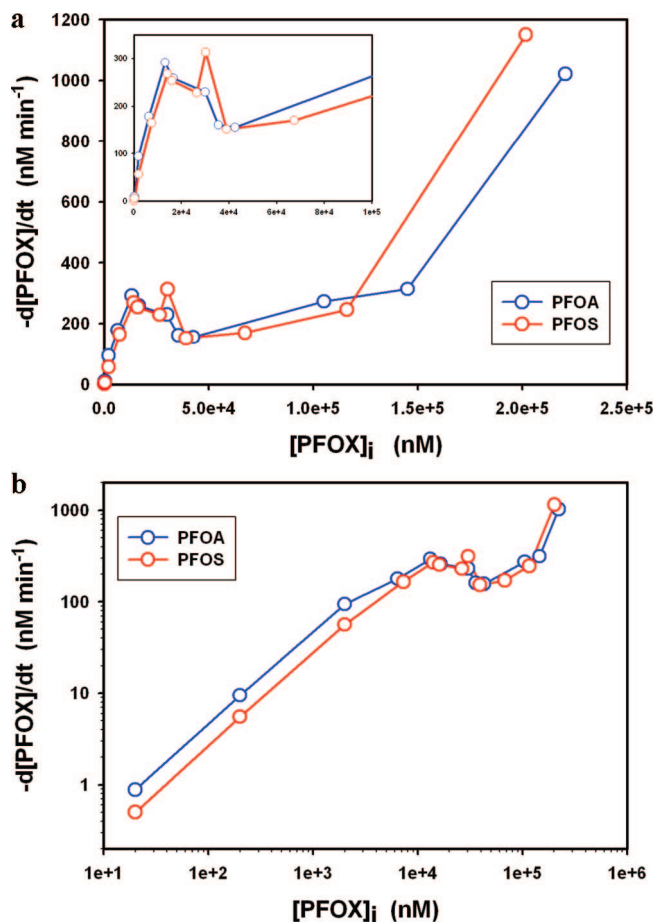


Figure 3. Absolute sonolytic degradation rate plotted as a function of initial PFOS and PFOA concentration. PFOS and PFOA were simultaneously degraded under ultrasonic conditions: 358 kHz, 250 W L⁻¹, 10 °C and argon. (red circles) PFOA and (blue circles) PFOS. (a) Linear–linear plot with the inset truncating off the final three data points. (b) Log–log plot.

order decay is similar to that observed for PFOS and consistent with saturation kinetics.

The observed kinetic parameters are given in Table 1. For low initial concentrations, $[\text{PFOX}]_i < 25 \mu\text{M}$ and $[\text{PFOX}]_i < 13 \mu\text{M}$, the time-dependent plot was fitted to an exponential curve to determine the first-order rate constant, $k_{\text{app}}^{-\text{PFOX}}$ (min^{-1}), and eq 1 was used to determine the absolute rate.

$$\frac{d[\text{PFOX}]}{dt} = -k_{\text{app}}^{-\text{PFOX}}[\text{PFOX}] \quad (1)$$

For high initial concentrations, $[\text{PFOX}]_i > 40 \mu\text{M}$, the time-dependent plot was fitted to a linear curve with the slope, $k_{\text{app}}^{-\text{PFOX}}$, taken to be the absolute degradation rate, eq 2.

$$\frac{d[\text{PFOX}]}{dt} = -k_{\text{app}}^{-\text{PFOX}} \quad (2)$$

For intermediate concentrations, the decay for the first 30 min was assumed to be linear and fit to eq 2, and the decay after 30 min was fit to eq 1. The overall degradation rate in Table 1 was taken as the temporal average of these two rates.

Equilibrium Partitioning to the Air–Water Interface. The Langmuir model describes adsorption to an interface. In the Langmuir model, the surface excess, Γ_{ex} , is a function of the equilibrium interface partitioning constant or surface activity, K_{eq} in liters per mole, and the maximum surface concentration Γ_{max} in moles per square meter. For example, equilibrium adsorption of PFOX to the air–water interface is modeled as shown in eq 3.

$$\Gamma_{\text{ex,eq}}^{\text{PFOX}} = \Gamma_{\text{Max,eq}}^{\text{PFOX}} \frac{K_{\text{eq}}^{\text{PFOX}}[\text{PFOX}]}{1 + K_{\text{eq}}^{\text{PFOX}}[\text{PFOX}]} \quad (3)$$

The corresponding $\Gamma_{\text{eq,ex}}^{\text{PFOX}}$ and $K_{\text{eq}}^{\text{PFOX}}$ values are determined from the dependence of surface tension on $[\text{PFOX}]$ (Figure 2) by least-squares fitting of the surface pressure to the Szyszkowski equation, eq 4.

$$\Pi = \gamma_0 - \gamma_{[\text{PFOX}]} = nRTT_{\text{Max,eq}}^{\text{PFOX}} \ln(1 + K_{\text{eq}}^{\text{PFOX}}[\text{PFOX}]) \quad (4)$$

where Π is the surface pressure in newtons per meter, $\gamma_0 = 0.072 \text{ N m}^{-1}$ is the surface tension of pure water, and $\gamma_{[\text{PFOX}]}$ is the surface tension at $[\text{PFOX}]$. Maximum air–water interface concentrations of $\Gamma_{\text{Max,eq}}^{\text{PFOA}} = 4.5 \times 10^{-6} \text{ mol m}^{-2}$ and $\Gamma_{\text{Max,eq}}^{\text{PFOS}} = 5.1 \times 10^{-6} \text{ mol m}^{-2}$ and equilibrium partitioning coefficients of $K_{\text{eq}}^{\text{PFOA}} = 360 \text{ L mol}^{-1}$ and $K_{\text{eq}}^{\text{PFOS}} = 1970 \text{ L mol}^{-1}$ are determined. The surface tension of solutions containing both PFOS and PFOA at equal concentrations was also measured and is plotted in Figure 2a. The stronger surfactant, PFOS, controls the surface tension as observed by the near overlap of the $\gamma_{[\text{PFOS}]}$ vs $[\text{PFOS}]$ curve and the $\gamma_{[\text{PFOS}] + [\text{PFOA}]}$ vs $[\text{PFOS}] + [\text{PFOA}]$ curve. Both the PFOS alone and $[\text{PFOS}] + [\text{PFOA}]$ curves truncate between 1 to 2 mM, as the sodium salt of PFOS becomes insoluble in water. However, the agreement $\Gamma_{\text{Max,eq}}^{\text{PFOX}}$ and $K_{\text{eq}}^{\text{PFOX}}$ values calculated here with previously determined values^{35–38} shows that solubility limits have minimal effect on the surface pressure fitting. Surface excess values versus $[\text{PFOX}]$ are plotted in Figure 2b; solid lines are for individual PFOX curves, and dashed lines are for individual components of the $[\text{PFOS}] + [\text{PFOA}]$ curve. A competitive adsorption isotherm was used to plot the $[\text{PFOS}] + [\text{PFOA}]$ surface excess values for each component. For example, eq 5 was used for PFOA.

$$\Gamma_{\text{ex,eq}}^{\text{PFOA}} = \Gamma_{\text{Max,eq}}^{\text{PFOA}} \frac{K_{\text{eq}}^{\text{PFOA}}[\text{PFOA}]}{1 + K_{\text{eq}}^{\text{PFOA}}[\text{PFOA}] + K_{\text{eq}}^{\text{PFOS}}[\text{PFOS}]} \quad (5)$$

PFOS is observed to be the dominant surfactant in Figure 2b,

as PFOA competition has little effect on the surface excess curve. In contrast, PFOA's surface excess curve under saturation conditions is shifted downward as PFOS outcompetes PFOA for air–water interface sites. The surface excess of PFOA under saturation conditions is decreased 7.2 times in the competitive curve (dashed) as compared to the noncompetitive curve (solid).

Discussion

$d[\text{PFOX}]/dt$ vs $[\text{PFOX}]_i$ Sonochemical Kinetic Modeling.

The transition from first-order to zero-order kinetics upon increasing the initial concentrations is consistent with saturation kinetics. Using the LH approach³⁹ to model $[\text{PFOX}]_i$ sonochemical kinetics, the absolute rate is proportional to $\theta_{\text{Sono}}^{\text{PFOX}}$, the fraction of total molecules adsorbed to the transiently cavitating bubble–water interface (eqs 6 and 7).

$$\theta_{\text{Sono}}^{\text{PFOX}} = \frac{K_{\text{Sono}}^{\text{PFOX}}[\text{PFOX}]}{1 + K_{\text{Sono}}^{\text{PFOX}}[\text{PFOX}]} \quad (6)$$

$$\frac{d[\text{PFOX}]}{dt} = -V_{\text{Max}}^{\text{PFOX}} \theta_{\text{Sono}}^{\text{PFOX}} \quad (7)$$

where $V_{\text{Max}}^{\text{PFOX}}$ (M s^{-1}) is the maximum reaction rate when all the available bubble surface sorption sites are occupied.

The transition in kinetic regimes is consistent with LH kinetic limits. At low PFOX concentration, when the surface is undersaturated and the observed kinetics are pseudo-first-order,

$$K_{\text{Sono}}^{\text{PFOX}}[\text{PFOX}] \ll 1 \quad (8)$$

$$\theta_{\text{Sono}}^{\text{PFOX}} = K_{\text{Sono}}^{\text{PFOX}}[\text{PFOX}] \quad (9)$$

$$\frac{d[\text{PFOX}]}{dt} = k_{\text{app}}^{-\text{PFOX}}[\text{PFOX}] = -V_{\text{Max}}^{\text{PFOX}} K_{\text{Sono}}^{\text{PFOX}}[\text{PFOX}] \quad (10)$$

$$k_{\text{app}}^{-\text{PFOX}} = -V_{\text{Max}}^{\text{PFOX}} K_{\text{Sono}}^{\text{PFOX}} \quad (11)$$

At intermediate concentration, there is a barrier to continued adsorption as the interfacial sites become increasingly populated (% levels):

$$\frac{d[\text{PFOX}]}{dt} = -V_{\text{Max}}^{\text{PFOX}} \frac{K_{\text{Sono}}^{\text{PFOX}}[\text{PFOX}]}{1 + K_{\text{Sono}}^{\text{PFOX}}[\text{PFOX}]} \quad (12)$$

At high concentration, all of the surface sites are occupied, and the maximum absolute rate is achieved:

$$K_{\text{Sono}}^{\text{PFOX}}[\text{PFOX}] \gg 1 \quad (13)$$

$$\frac{d[\text{PFOX}]}{dt} = -V_{\text{Max}}^{\text{PFOX}} \quad (14)$$

Thus, at low and intermediate concentration, the kinetics are controlled by the fraction of the total PFOX molecules adsorbed to the bubble–water interface, as given by the Langmuir isotherm (eq 6). At high concentration, the bubble–water interface is saturated with PFOX molecules, and the rate is limited by the intrinsic chemical reaction rate (e.g., PFOX pyrolysis).^{40–45}

Figure 3a,b plots the PFOX absolute degradation rate vs $[\text{PFOX}]_i$ in linear–linear and log–log format, respectively (values from Table 1). Over the initial concentration range, $20 \text{ nM} < [\text{PFOX}]_i < 2000 \text{ nM}$, $k_{\text{app}}^{-\text{PFOX}}$ (eq 1) are constant: $k_{\text{app}}^{-\text{PFOA}} = 0.047 \text{ min}^{-1}$, $k_{\text{app}}^{-\text{PFOS}} = 0.028 \text{ min}^{-1}$, and $k_{\text{app}}^{-\text{PFOA}} = 1.68 k_{\text{app}}^{-\text{PFOS}}$. This indicates that the surface is undersaturated, and the observed increase in absolute rate is due to the increasing

TABLE 2: Sonochemical vs Equilibrium Surface Activity

	frequency (kHz)	applied power density (W L ⁻¹)	$\Gamma_{\text{eq,max}}^{\text{PFOA}}$ (mol m ⁻²)	$K_{\text{eq}}^{\text{PFOA}}$ (M ⁻¹)	$V_{\text{sono,max}}^{\text{PFOA}}$	$K_{\text{Sono}}^{\text{PFOA}}$ (M ⁻¹)	$K_{\text{Sono}}^{\text{PFOA}}/K_{\text{Eq}}^{\text{PFOA}}$	ref
PFOS	354	250	5.1e-6	1970	230 nM min ⁻¹	121000	60	this work
PFOA	354	250	4.5e-6	360	1660 nM min ⁻¹	28500	80	this work
SDS	47		6.9e-6 ⁵²	40052	1 μM min ⁻¹	5000	12.5	31
SOS	47		6.4e-6 ⁵²	2252	1.4 μM min ⁻¹	8000	410	31
Humic	20	14000	4.6e-6 ⁵³	1180 ⁵³		4e6	3400	29

$\theta_{\text{Sono}}^{\text{PFOA}}$. However, at similar bulk concentrations, PFOS is expected to have a greater equilibrium activity at the bubble–water interface, even though the maximum interfacial concentrations are similar, $\Gamma_{\text{max}}^{\text{PFOA}} = 1.1\Gamma_{\text{max}}^{\text{PFOS}}$, because PFOS has a larger partitioning coefficient, $K_{\text{eq}}^{\text{PFOS}} = 5.5 K_{\text{eq}}^{\text{PFOA}}$. Thus the theoretical sonochemical degradation rate for PFOA is greater than that for PFOS or $V_{\text{Max,Theo}}^{\text{PFOA}} > V_{\text{Max,Theo}}^{\text{PFOS}}$, and if $\theta_{\text{Sono}}^{\text{PFOS}} > \theta_{\text{Sono}}^{\text{PFOA}}$, then $V_{\text{Max,Theo}}^{\text{PFOA}}/V_{\text{Max,Theo}}^{\text{PFOS}} > \theta_{\text{Sono}}^{\text{PFOS}}/\theta_{\text{Sono}}^{\text{PFOA}}$. Given that $k_{\text{app}}^{\text{PFOA}} = 1.68 k_{\text{app}}^{\text{PFOS}}$ (eq 11) and $K_{\text{eq}}^{\text{PFOA}}/K_{\text{eq}}^{\text{PFOS}} = 5.5$, the theoretical ratio $V_{\text{Max,Theo}}^{\text{PFOA}}/V_{\text{Max,Theo}}^{\text{PFOS}}$ is determined to be 9.3 under current ultrasonic conditions.

At initial concentrations over the range of $13 \mu\text{M} < [\text{PFOA}]_i < 150 \mu\text{M}$, PFOS and PFOA absolute rates are observed to saturate at $V_{\text{Max,App}}^{\text{PFOA}} = 240 \pm 60 \text{ nM min}^{-1}$ and $V_{\text{Max,App}}^{\text{PFOS}} = 230 \pm 60 \text{ nM min}^{-1}$, confirming that the bubble–water interface is saturated. Convergence of $V_{\text{Max,App}}^{\text{PFOA}}$ and $V_{\text{Max,App}}^{\text{PFOS}}$ is at variance with relative kinetics at low concentrations. Under saturation conditions, PFOS as the stronger surfactant should out-compete PFOA for bubble surface sites and is thus able to compensate for the difference in the theoretical maximum pyrolytic rate constants causing the apparent rates to converge. This is consistent with equilibrium partitioning where PFOS competition decreased the PFOA maximum surface excess by a factor of 7.2 (Figure 2b). If PFOA were to be sonolytically degraded in the absence of PFOS, it would be expected to have a maximum degradation rate approximately 9.3 times greater than the experimentally observed rate or $V_{\text{Max}}^{\text{PFOA}} = 2230 \pm 560 \text{ nM min}^{-1}$. The determined $V_{\text{Max}}^{\text{PFOA}}$ values, low concentration $k_{\text{app}}^{\text{PFOA}}$ and eq 11 are used to calculate $K_{\text{Sono}}^{\text{PFOA}}$ values of $K_{\text{Sono}}^{\text{PFOA}} = 121\,000 \text{ M}^{-1}$ and $K_{\text{Sono}}^{\text{PFOA}} = 28\,500 \text{ M}^{-1}$. Both values are greater than equilibrium air–water interface partitioning values yielding relative sonochemical to equilibrium surface activities of $K_{\text{Sono}}^{\text{PFOA}}/K_{\text{Eq}}^{\text{PFOA}} = 60$ and $K_{\text{Sono}}^{\text{PFOA}}/K_{\text{Eq}}^{\text{PFOA}} = 80$ (Table 2).

The absolute PFOS degradation rates are modeled using the competitive LH model (eq 15), as shown in Figure 4, where $V_{\text{Max}}^{\text{PFOS}}$ is set to the empirically determined value $V_{\text{Max,app}}^{\text{PFOS}} = 230 \text{ nM min}^{-1}$ and $K_{\text{Sono}}^{\text{PFOS}}$ is set equal to $K_{\text{Eq}}^{\text{PFOS}}$ (black line), $10 \times K_{\text{Eq}}^{\text{PFOS}}$ (blue line), and $100 \times K_{\text{Eq}}^{\text{PFOS}}$ (red line); $K_{\text{Eq}}^{\text{PFOA}}$ was adjusted accordingly.

$$\frac{d[\text{PFOS}]}{dt} = -V_{\text{Max}}^{\text{PFOS}} \frac{K_{\text{Sono}}^{\text{PFOS}}[\text{PFOS}]}{1 + K_{\text{Sono}}^{\text{PFOA}}[\text{PFOA}] + K_{\text{Sono}}^{\text{PFOS}}[\text{PFOS}]} \quad (15)$$

The primary plots of Figure 4 are in log–log format, while the inset is in linear–linear format. The best fit to the experimental data (black dots) is obtained when $K_{\text{Sono}}^{\text{PFOS}} = 100 \times K_{\text{Eq}}^{\text{PFOS}}$. PFOA surface competition had little effect on the fit as the noncompetitive LH model yields a similar result (Figure S1, Supporting Information). Altering $V_{\text{Max}}^{\text{PFOS}}$ rather than $K_{\text{Sono}}^{\text{PFOS}}$ does not improve the fitting of the LH model to the experimental data (Figure S2, Supporting Information).

Applying the LH formalism to PFOA sonochemical kinetics is slightly more difficult since it is the weaker surfactant, and competitive adsorption will have a more prominent effect

(Figure 2). In Figure 5a, the absolute PFOA degradation rate versus initial PFOA concentration is modeled using the competitive LH formalism, eq 16, with $V_{\text{Max}}^{\text{PFOA}}$ set to the empirically determined 240 nM min^{-1} , and $K_{\text{Sono}}^{\text{PFOA}}$ is set equal to $K_{\text{Eq}}^{\text{PFOA}}$ (black line), $10 \times K_{\text{Eq}}^{\text{PFOA}}$ (blue line), and $100 \times K_{\text{Eq}}^{\text{PFOA}}$ (red line); $K_{\text{Eq}}^{\text{PFOA}}$ is adjusted accordingly.

$$\frac{d[\text{PFOA}]}{dt} = -V_{\text{Max}}^{\text{PFOA}} \frac{K_{\text{Sono}}^{\text{PFOA}}[\text{PFOA}]}{1 + K_{\text{Sono}}^{\text{PFOA}}[\text{PFOA}] + K_{\text{Sono}}^{\text{PFOS}}[\text{PFOS}]} \quad (16)$$

The model calculations underestimate the experimental data by at least an order of magnitude in both the surface-saturated and undersaturated regimes. In Figure 5b, $V_{\text{Max}}^{\text{PFOA}}$ is set to 2230 nM min^{-1} , as calculated using the relationship $V_{\text{Max,Theo}}^{\text{PFOA}}/V_{\text{Max,Theo}}^{\text{PFOS}} = 9.3$ to account for PFOS outcompeting PFOA for bubble interface adsorption sites. When $K_{\text{Sono}}^{\text{PFOA}} = 100 \times K_{\text{Eq}}^{\text{PFOA}}$, the best qualitative fit to the experimental data is obtained. $d[\text{PFOA}]/dt$ vs $[\text{PFOA}]_i$ fits for noncompetitive LH models are provided in the Supporting Information. With $V_{\text{Max}}^{\text{PFOA}} = 240 \text{ nM min}^{-1}$ and $K_{\text{Sono}}^{\text{PFOA}} = 1000 \times K_{\text{Eq}}^{\text{PFOA}}$, a good data fit is obtained, while, at $V_{\text{Max}}^{\text{PFOA}} = 2230 \text{ nM min}^{-1}$, none of the models result in a good fit to the data (Figures S3 and S4, respectively).

As $[\text{PFOA}]_i$ increases to greater than $200 \mu\text{M}$, $d[\text{PFOA}]/dt$ increases substantially to $>1000 \text{ nM min}^{-1}$, at variance with the LH kinetic model. Previous reports on ionic surfactant sonochemistry provide insight into this phenomenon. Ashokkumar et al.⁴⁶ observed that, upon increasing aqueous SDS concentration, SL increased, reaching a maximum at $[\text{SDS}] = 1 \text{ mM}$. The increase in SL was attributed to SDS accumulation and thus build-up of charge on the bubble surface. Electrostatic repulsion between charged bubbles reduced bubble clustering, leading to a greater number of more intense SL active bubble

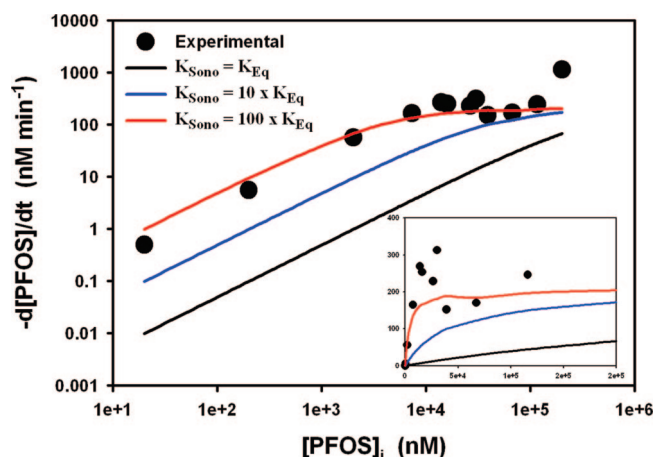


Figure 4. Absolute PFOS sonolytic degradation rate plotted as a function of initial PFOS concentration fitted by the competitive LH model, eq 15: $V_{\text{Max}}^{\text{PFOS}} = 230 \text{ nM min}^{-1}$. (●) experimental, (black line) $K_{\text{Sono}}^{\text{PFOS}} = K_{\text{Eq}}^{\text{PFOS}}$, (blue line) $K_{\text{Sono}}^{\text{PFOS}} = 10 \times K_{\text{Eq}}^{\text{PFOS}}$, and (red line) $K_{\text{Sono}}^{\text{PFOS}} = 100 \times K_{\text{Eq}}^{\text{PFOS}}$.

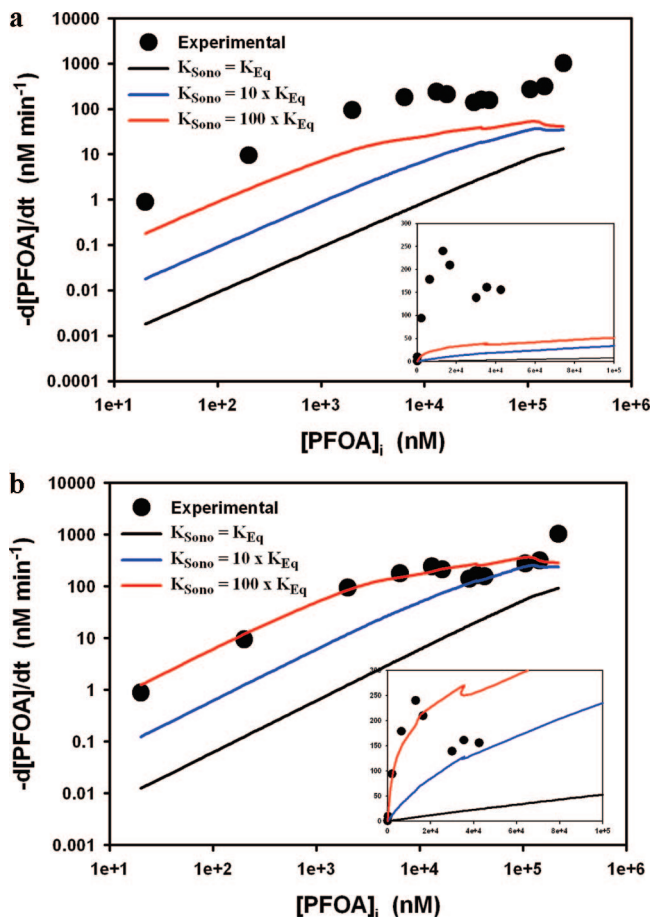


Figure 5. Absolute PFOS sonolytic degradation rate plotted as a function of initial PFOA concentration fitted by the competitive LH model, eq 16: (a) $V_{\text{Max}}^{\text{PFOA}} = 240 \text{ nM min}^{-1}$ and (b) $V_{\text{Max}}^{\text{PFOA}} = 2230 \text{ nM min}^{-1}$. (●) experimental; (black line) $K_{\text{Sono}}^{\text{PFOA}} = K_{\text{Eq}}^{\text{PFOA}}$; (blue line) $K_{\text{Sono}}^{\text{PFOA}} = 10 \times K_{\text{Eq}}^{\text{PFOA}}$; and (red line) $K_{\text{Sono}}^{\text{PFOA}} = 100 \times K_{\text{Eq}}^{\text{PFOA}}$.

events. Total bubble volume was reported to decrease as bulk [SDS] was increased, with a 50% reduction in total bubble volume at [SDS] = $100 \mu\text{M}$,⁴⁷ suggesting a reduction in bubble coalescence. Increasing [SDS] led to a decrease in broadband acoustic emission, even though total acoustic emission increased,⁴⁸ suggesting a transition to a greater number of more intense bubble collapse events⁴⁹ due to reduction in bubble–bubble clustering and coalescence. As anionic surfactants, PFOS and PFOA would be expected to have a similar effect on bubble–bubble interactions as SDS. The increase in PFOX absolute degradation rate occurs at $[\text{PFOX}]_i > 100 \mu\text{M}$, consistent with SDS concentrations where SL, total bubble volume, and acoustic emission effects are observed to take effect. Reduction in bubble–bubble coalescence and clustering leading to a greater number of more intense bubble collapse events would result in a greater number of bubble interface face adsorption sites and, consequently, an increase in PFOX sonochemical degradation kinetics.

Nonequilibrium Bubble Surface Activity. Optimized fitting of the experimental kinetic data as a function of [PFOX] to the LH model gives $K_{\text{Sono}}^{\text{PFOS}} = 60 K_{\text{Eq}}^{\text{PFOS}}$ and $K_{\text{Sono}}^{\text{PFOA}} = 80 K_{\text{Eq}}^{\text{PFOA}}$. Data from two previous reports, which is fit to LH kinetics, is presented in Table 2. Concentration-dependent alkyl radical production for SDS and sodium octyl sulfate (SOS) from the work of Sostaric and Reisz³¹ was fit to the LH model using an empirically determined maximum rate of alkyl radical production. For both compounds, K_{Sono} appears to be greater than K_{Eq} . The relative difference between K_{Sono} and K_{Eq} was greater for

the weaker surfactant: $K_{\text{Sono}}^{\text{SDS}} = 12.5 K_{\text{Eq}}^{\text{SDS}}$ vs $K_{\text{Sono}}^{\text{SOS}} = 410 K_{\text{Eq}}^{\text{SOS}}$. This trend is expected to hold for sodium pentyl sulfonate (SPSo), a weaker surfactant than SOS, which had a similar sonochemical surface activity to that of SOS and SDS. Kim and Jung²⁹ modeled sonochemical degradation of humic acids (anionic, surface-active natural organic matter) with LH kinetics, and their results give values of $K_{\text{Sono}} > K_{\text{Eq}}$ as well. The humic acid degradation kinetics gave the greatest relative surface activity difference, $K_{\text{Sono}}^{\text{Humic}} = 3400 K_{\text{Eq}}^{\text{Humic}}$ that was most likely due to the very high applied acoustic power density, $14\,000 \text{ W L}^{-1}$.

Greater sonochemical surface activity over that of the predicted equilibrium surface activity was predicted by the calculations of Fryllis and Szeri.²⁸ Their work argues that high velocity bubble oscillations should increase the transport of surfactants to a lightly populated surface. Their conclusions are in qualitative agreement with the work of Eller and Flynn⁵⁰ on rectified diffusion. Under their “high frequency approximation”, which is valid for $f > 20 \text{ kHz}$, diffusion can be assumed to be a slow process as compared to the radial motion of acoustic bubbles. For example, the sonochemical surface activity can be broken in the ratio of the rates of adsorption to and desorption from the interface: $K_{\text{Sono}} = k_{\text{ads}}/k_{\text{des}}$. Thus an increase in k_{ads} or a decrease in k_{des} will result in an increase in K_{Sono} . It is much easier to rationalize an increase in k_{ads} . For a lightly populated surface, $k_{\text{ads}} = k_{\text{dif}}$, and processes such as high velocity bubble oscillations or acoustic microstreaming may enhance diffusion to the bubble interface. A rough, yet insightful example will be presented to further this point.

A transiently cavitating bubble will expand from its average initial radius, R_0 , to its max radius, R_{max} , over a period of $0.5f$ where f is the ultrasonic frequency.¹⁹ R_{max} (μm) can be calculated using the equation

$$R_{\text{max}}(\mu\text{m}) = (3 \times 10^6/f)(P_a - 1)(P_a)^{-1/2}[1 + 2(P_a - 1)/3]^{1/3} \quad (17)$$

where P_a is the acoustic pressure, $P_a = (2\rho C_L I_A)^{1/2}/101\,325 \text{ bar}$, ρ is the density of water (1000 kg m^{-3}), C_L is the speed of sound in water (1500 m s^{-1}), and I_A is the acoustic intensity ($51\,000 \text{ W m}^{-2}$ at a calorimetric power of 120 W over a transducer area of 23.5 cm^2). Assuming a monotonic distribution of bubbles,⁵¹ R_0 can be estimated as the average of $R_{\text{max}}/2.5$, which is the dynamic limit for transient cavitation, and R_B is Blake’s radius of bubble dissolution.¹⁹ Since $R_B \ll R_{\text{max}}/2.5$, the value of R_0 is roughly $R_{\text{max}}/5$. Sonochemical parameters of 354 kHz and 120 W correspond to $R_{\text{max}} = 18 \mu\text{m}$ and $R_{\text{max}}/5 = 3.6 \mu\text{m}$. Thus, a point on the bubble surface travels a radial distance of $14.4 \mu\text{m}$ over the rarefaction period of $1.2 \mu\text{s}$, and, assuming a constant radial velocity, a point at the bubble surface will travel at 12 m s^{-1} during expansion under the present sonochemical conditions. If we assume a diffusion constant of $10^{-5} \text{ cm}^2 \text{ s}^{-1}$ or $10^{-3} \mu\text{m}^2 \mu\text{s}^{-1}$ for PFOS and PFOA, over a period of $1.2 \mu\text{s}$, a single molecule is expected to travel around 35 nm , which is much less than the bubble radial motion of $14.4 \mu\text{m}$ over the same period.

The differential volume between the average initial bubble, $R_0 = 3.6 \mu\text{m}$, and a bubble at its maximum radius, $R_{\text{max}} = 18 \mu\text{m}$, is $V_{\text{diff}} = (4/3)\pi(18^3 - 3.6^3) = 24\,200 \mu\text{m}^3$. Using the high-frequency assumption that the rate of diffusion is significantly less than the rate of radial expansion, then all of the PFOS or PFOA molecules contained in the initial volume would be packed into a sheath of 35 nm in radius around the maximal bubble volume, $V_{\text{sheath}} = (4/3)\pi(18.035^3 - 18^3) = 143 \mu\text{m}^3$.

The ratio of the initial differential bubble volume to the bubble sheath volume, $V_{\text{diff}}/V_{\text{sheath}}$, is 170. This suggests that the sonochemically induced increase in PFOS and PFOA surface activity may be partially due to high velocity bubble oscillations enhancing the diffusion of the FCs to the bubble–water interface. Other effects such as acoustic microstreaming²⁴ may also be responsible for enhanced diffusion to the bubble interface and thus the sonochemical surface activity.

The results here are seemingly at variance with recent work by Tronson et al.³³ and Sunartio et al.,³⁴ which concluded that the Gibb's surface excess was not attained for nonvolatile surfactants. Fyrrillas and Szeri²⁸ predicted that high-velocity bubble oscillations would reduce the maximal surfactant bubble surface population. This is consistent with conclusions that relatively short acoustic bubble lifetimes (ca. 100 μs) as compared to ionic surfactant equilibration times (>1 ms) led to the Gibb's surface excess not being attained during ultrasonic irradiation. Examples of possible nonequilibrium sonochemical PFOS surface activities, K^{PFOS} , and possible nonequilibrium sonochemical max surface excesses, $\Gamma_{\text{Max}}^{\text{PFOS}}$, and their affects on the surface excess population, $\Gamma_{\text{ex}}^{\text{PFOS}}$ (eq. 3), are presented in Figure 6. Variations in $\Gamma_{\text{Max}}^{\text{PFOS}}$ lead to a vertical shift in the $\Gamma_{\text{ex}}^{\text{PFOS}}$ vs [PFOS] curve, with the expected sonochemical effect to be a decrease in $\Gamma_{\text{Max}}^{\text{PFOS}}$ and thus an overall, concentration-independent decrease in $\Gamma_{\text{ex}}^{\text{PFOS}}$. Variations in K^{PFOS} lead to a horizontal shift in the $\Gamma_{\text{ex}}^{\text{PFOS}}$ vs [PFOS] curves. The experimental results presented here suggest an increase in K^{PFOS} and thus a shift in the direction of the ordinate. If a decrease in $\Gamma_{\text{Max}}^{\text{PFOS}}$ and an increase in K^{PFOS} occur upon moving from equilibrium air–water interface partitioning to a sonochemical air–water interface partitioning, then, under surface saturation conditions, a decrease in $\Gamma_{\text{ex}}^{\text{PFOS}}$ would still be predicted. Therefore, the experimental results presented suggesting a sonochemical increase in surface activity, $K_{\text{Sono}} > K_{\text{Eq}}$, are not necessarily at variance with previous results suggesting the Gibb's surface excess was not attained for nonvolatile solutes. For example, in Figure 6c, simultaneous variations in both $\Gamma_{\text{Max}}^{\text{PFOS}}$ and K^{PFOS} have been plotted. Decreasing $\Gamma_{\text{Max}}^{\text{PFOS}}$ by a factor of 10 also reduces $\Gamma_{\text{ex}}^{\text{PFOS}}$ under lightly populated conditions by a factor of 10 (green line). Increasing K^{PFOS} by a factor of 10 (blue line) brings $\Gamma_{\text{ex}}^{\text{PFOS}}$ to the equilibrium level (black line) for undersaturation conditions. Furthermore, when $\Gamma_{\text{Max}}^{\text{PFOS}}$ is decreased by a factor of 10 and K^{PFOS} is increased by a factor of 100 (red line), the $\Gamma_{\text{ex}}^{\text{PFOS}}$ then exceeds the predicted equilibrium adsorption limit for lightly populated conditions and is still below predicted equilibrium adsorption for saturation conditions.

Conclusions

The sonochemical degradation kinetics of PFOS and PFOA have been studied over the concentration range of 20 nM $<$ [PFOX]_i $<$ 200 μM . The kinetics are fit to the LH model using experimental rate maximums of $V_{\text{Max}}^{\text{PFOA}} = 2230 \pm 560$ nM min⁻¹ and $V_{\text{Max}}^{\text{PFOS}} = 230 \pm 60$ nM min⁻¹. The corresponding sonochemical bubble surface activities for PFOS and PFOA are determined to be $K_{\text{Sono}}^{\text{PFOS}} = 120\,000$ M⁻¹ and $K_{\text{Sono}}^{\text{PFOA}} = 28\,500$ M⁻¹, respectively. Competitive bubble surface adsorption is factored into the LH model in order to accurately model the kinetics of PFOA under saturation conditions. The sonochemical surface activities, $K_{\text{Sono}}^{\text{PFOX}}$, are 50 to 100 times greater than the predicted equilibrium air–water interfacial activities, $K_{\text{Eq}}^{\text{PFOX}}$, as determined via concentration-dependent surface tension measurements. The apparent enhancements in bubble surface activities has positive implications for the application of ultrasonic irradiation as a treatment technology for dilute (<1

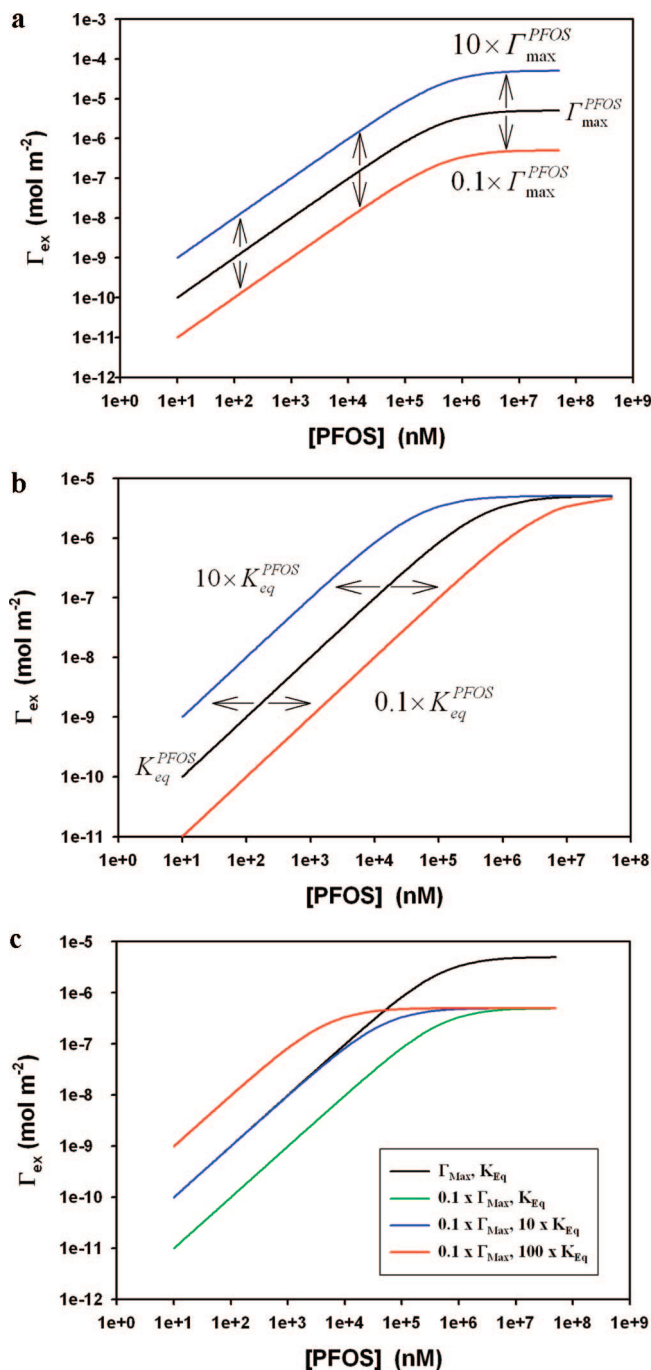


Figure 6. PFOS surface excess vs PFOS bulk concentration, eq 5: (a) (black line) $\Gamma_{\text{Max}}^{\text{PFOS}}$, (blue line) $10 \times \Gamma_{\text{Max}}^{\text{PFOS}}$, and (red line) $0.1 \times \Gamma_{\text{Max}}^{\text{PFOS}}$; (b) (black line) $K_{\text{Eq}}^{\text{PFOS}}$, (blue line) $10 \times K_{\text{Eq}}^{\text{PFOS}}$, and (red line) $0.1 \times K_{\text{Eq}}^{\text{PFOS}}$; and (c) (black line) $\Gamma_{\text{Max}}^{\text{PFOS}}$ and $K_{\text{Eq}}^{\text{PFOS}}$, (green line) $0.1 \times \Gamma_{\text{Max}}^{\text{PFOS}}$ and $K_{\text{Eq}}^{\text{PFOS}}$, (blue line) $0.1 \times \Gamma_{\text{Max}}^{\text{PFOS}}$ and $10 \times K_{\text{Eq}}^{\text{PFOS}}$, and (red line) $0.1 \times \Gamma_{\text{Max}}^{\text{PFOS}}$ and $100 \times K_{\text{Eq}}^{\text{PFOS}}$.

μM) aqueous solutions of PFOS and PFOA. At low concentrations, the efficacy of conventional chemical treatment methods is greatly reduced as a result of concentration effects. These results will also have implications for the sonochemical destruction of other pollutants where adsorption to the transiently cavitating bubble interface is expected to partially mediate absolute degradation rates.

Acknowledgment. We would like to thank the 3M Company for research support. This support included the donation to Caltech of analytical standards and an Agilent LC-MS-Ion Trap

mass spectrometer. The authors also thank Dr. Nathan Dalleska of the Environmental Analytical Center.

Supporting Information Available: Alternative LH fittings of the experimental data. This material is available free of charge via the Internet at <http://pubs.acs.org>.

References and Notes

- (1) 3M Company. *The Science of Organic Fluorochemistry*; Docket AR226-0547; Office of Pollution Prevention and Toxics, U.S. Environmental Protection Agency: Washington, DC, 1999; p 12.
- (2) 3M Company. *Sulfonated Perfluorochemicals in the Environment: Sources, Dispersion, Fate and Effects*; Docket AR226-0620; Office of Pollution Prevention & Toxics, U.S. Environmental Protection Agency: Washington, DC, 2000; p 51.
- (3) Vecitis, C. D.; Park, H.; Cheng, J.; Mader, B. T.; Hoffmann, M. R. *J. Phys. Chem. A* **2008**, *112*, 4261.
- (4) Key, B. D.; Howell, R. D.; Criddle, C. S. *Environ. Sci. Technol.* **1998**, *32*, 2283.
- (5) Schultz, M. M.; Higgins, C. P.; Huset, C. A.; Luthy, R. G.; Barofsky, D. F.; Field, J. A. *Environ. Sci. Technol.* **2006**, *40*, 7350.
- (6) Schroder, H. F.; Meesters, R. J. W. *J. Chromatogr. A* **2005**, *1082*, 110.
- (7) Hori, H.; Yamamoto, A.; Hayakawa, E.; Taniyasu, S.; Yamashita, N.; Kutsuna, S.; Kiatagawa, H.; Arakawa, R. *Environ. Sci. Technol.* **2005**, *39*, 2383.
- (8) Chen, J.; Zhang, P. *Water Sci. Technol.* **2006**, *54*, 317.
- (9) Hori, H.; Hayakawa, E.; Einaga, H.; Kutsuna, S.; Koike, K.; Ibusuki, T.; Kiatagawa, H.; Arakawa, R. *Environ. Sci. Technol.* **2004**, *38*, 6118.
- (10) Hori, H.; Nagaoka, Y.; Yamamoto, A.; Sano, T.; Yamashita, N.; Taniyasu, S.; Kutsuna, S.; Osaka, I.; Arakawa, R. *Environ. Sci. Technol.* **2006**, *40*, 1049.
- (11) Yamamoto, T.; Noma, Y.; Sakai, S. I.; Shibata, Y. *Environ. Sci. Technol.* **2007**, *41*, 5660.
- (12) Hori, H.; Hayakawa, E.; Koike, K.; Einaga, H.; Ibusuki, T. *J. Mol. Catal. A: Chem.* **2004**, *211*, 35.
- (13) Dillert, R.; Bahnemann, D.; Hidaka, H. *Chemosphere* **2007**, *67*, 785.
- (14) Moriwaki, H.; Takagi, Y.; Tanaka, M.; Tsuruho, K.; Okitsu, K.; Maeda, Y. *Environ. Sci. Technol.* **2005**, *39*, 3388.
- (15) Jennings, B. H.; Townsend, S. N. *J. Phys. Chem.* **1961**, *65*, 1574.
- (16) Destailats, H.; Hung, H. M.; Hoffmann, M. R. *Environ. Sci. Technol.* **2000**, *34*, 311.
- (17) Kotronarou, A.; Mills, G.; Hoffmann, M. R. *J. Phys. Chem.* **1991**, *95*, 3630.
- (18) Petrier, C.; David, B.; Laguian, S. *Chemosphere* **1996**, *32*, 1709.
- (19) Brennen, C. E. *Cavitation and Bubble Dynamics*; Oxford University Press: New York, 1995.
- (20) Didenko, Y. T.; McNamara, W. B.; Suslick, K. S. *J. Am. Chem. Soc.* **1999**, *121*, 5817.
- (21) Ciawi, E.; Rae, J.; Ashokkumar, M.; Grieser, F. *J. Phys. Chem. B* **2006**, *110*, 13656.
- (22) Ashokkumar, M.; Grieser, F. *J. Am. Chem. Soc.* **2005**, *127*, 5326.
- (23) Eddingsaas, N. C.; Suslick, K. S. *J. Am. Chem. Soc.* **2007**, *129*, 3838.
- (24) Leighton, T. G. *The Acoustic Bubble*; Academic Press: London, 1994.
- (25) Hung, H. M.; Hoffmann, M. R. *J. Phys. Chem. A* **1999**, *103*, 2734.
- (26) Vecitis, C. D.; Park, H.; Cheng, J.; Mader, B. M.; Hoffmann, M. R. *J. Phys. Chem. A* **2008**, *112*, 4261.
- (27) Henglein, A.; Kormann, C. *Int. J. Radiat. Biol.* **1985**, *48*, 251.
- (28) Fyrrillas, M. M.; Szeri, A. J. *J. Fluid Mech.* **1996**, *311*, 361.
- (29) Kim, I. K.; Jung, O. J. *Bull. Korean Chem. Soc.* **2001**, *22*, 1093.
- (30) O'Shea, K. E.; Aguila, A.; Vinodgopal, K.; Kamat, P. V. *Res. Chem. Intermed.* **1998**, *24*, 695.
- (31) Sostaric, J. Z.; Riesz, P. J. *Am. Chem. Soc.* **2001**, *123*, 11010.
- (32) Sostaric, J. Z.; Riesz, P. J. *Phys. Chem. B* **2002**, *106*, 12537.
- (33) Tronson, R.; Ashokkumar, M.; Grieser, F. *J. Phys. Chem. B* **2003**, *107*, 7307.
- (34) Sunartio, D.; Ashokkumar, M.; Grieser, F. *J. Am. Chem. Soc.* **2007**, *129*, 6031.
- (35) Lopez-Fontan, J. L.; Gonzalez-Perez, A.; Costa, J.; Ruso, J. M.; Prieto, G.; Schulz, P. C.; Sarmiento, M. *J. Colloid Interface Sci.* **2006**, *294*, 458.
- (36) Lopez-Fontan, J. L.; Sarmiento, F.; Schulz, P. C. *Colloid Polym. Sci.* **2005**, *283*, 862.
- (37) Simister, E. A.; Lee, E. M.; Lu, J. R.; Thomas, R. K.; Ottewill, R. H.; Rennie, A. R.; Penfold, J. J. *Chem. Soc., Faraday Trans.* **1992**, *88*, 3033.
- (38) Shinoda, K.; Hato, M.; Hayashi, T. *J. Phys. Chem.* **1972**, *76*, 909.
- (39) Langmuir, I. *J. Am. Chem. Soc.* **1916**, *38*, 2221.
- (40) Glockner, V.; Lunkwitz, K.; Prescher, D. *Tenside, Surfactants, Deterg.* **1989**, *26*, 376.
- (41) Lines, D.; Sutcliffe, H. *J. Fluor. Chem.* **1984**, *25*, 505.
- (42) Lazerte, J. D.; Hals, L. J.; Reid, T. S.; Smith, G. H. *J. Am. Chem. Soc.* **1953**, *75*, 4525.
- (43) Hals, L. J.; Reid, T. S.; Smith, G. H. *J. Am. Chem. Soc.* **1951**, *73*, 4054.
- (44) Krusic, P. J.; Marchione, A. A.; Roe, D. C. *J. Fluor. Chem.* **2005**, *126*, 1510.
- (45) Krusic, P. J.; Roe, D. C. *Anal. Chem.* **2004**, *76*, 3800.
- (46) Ashokkumar, M.; Hall, R.; Mulvaney, P.; Grieser, F. *J. Phys. Chem. B* **1997**, *101*, 10845.
- (47) Lee, J.; Kentish, S. E.; Ashokkumar, M. *J. Phys. Chem. B* **2005**, *109*, 5095.
- (48) Ashokkumar, M.; Hodnett, M.; Zeqiri, B.; Grieser, F.; Price, G. J. *J. Am. Chem. Soc.* **2007**, *129*, 2250.
- (49) Price, G. J.; Ashokkumar, M.; Hodnett, M.; Zequiri, B.; Grieser, F. *J. Phys. Chem. B* **2005**, *109*, 17799.
- (50) Eller, A.; Flynn, H. G. *J. Acoust. Soc. Am.* **1965**, *37*, 493.
- (51) Colussi, A. J.; Hung, H. M.; Hoffmann, M. R. *J. Phys. Chem. A* **1999**, *103*, 2696.
- (52) Lunkenheimer, K.; Czichocki, G.; Hirte, R.; Barzyk, W. *Colloid Surf. A: Physicochem. Eng. Aspects* **1995**, *101*, 187.
- (53) Tuckermann, R. *Atmos. Environ.* **2007**, *41*, 6265.